Combined Source-Channel Coding of Images

JAMES W. MODESTINO, MEMBER, IEEE, AND DAVID G. DAUT, STUDENT MEMBER, IEEE

Abstract—**A combined source-channel coding approach is described for the encoding, transmission and remote reconstruction of image data. The source encoder employs two-dimensional (2-D) differential pulse code modulation (DPCM). This is a relatively efficient encoding scheme in the absence of channel errors. In the presence of channel errors, however, the performance degrades rapidly. By providing error control protection to those encoded bits which contribute most significantly to image reconstruction, it is possible to minimize this degradation without sacrificing transmission bandwidth. The result is a relatively robust design which is reasonably insensitive to channel errors and yet provides performance approaching the rate-distortion bound. Analytical results are provided for assumed 2-D autoregressive image models while simulation results are described for real-world images.**

I. INTRODUCTION

THERE has been widespread interest recently in the efficient encoding of image data. Two-dimensional (2-D) differential pulse code modulation (DPCM) is a technique which has been widely employed for this purpose. Its behavior in the absence of channel errors has been studied extensively and is well-documented [1]-[5]. In the presence of channel errors, however, the behavior of 2-D DPCM degrades rapidly. Indeed, on some fairly representative channels, increasing the quantization accuracy degrades rather than improves the subjective reconstructed image quality. As a result, some form of error control protection must be provided if high-quality image reconstruction is to be achieved. Since channel coding generally entails a bandwidth expansion, this operation can be extremely wasteful of channel bandwidth unless applied judiciously. In particular, tradeoffs must be made between the reconstruction accuracy associated with the source coder and the degree of error control protection provided by the channel coding.

In this paper we describe a combined source-channel coding approach for the encoding, transmission and remote reconstruction of image data which exploits these tradeoffs. The source encoder employs 2-D DPCM which has been appropriately matched to the image source. By providing selective error control protection to those bits which contribute most significantly to image reconstruction, it is possible to significantly improve the reconstructed image quality without sacrificing transmission bandwidth. The result is a relatively robust design which is reasonably insensitive to channel errors and yet provides performance approaching an achievable rate-distortion bound. While the primary motivation for this work was 2-D image coding, we expect that the results have application to coding of 1-D sources as well.

The overall 2-D DPCM system is described in Section II and includes typical performance results without channel coding. An analysis of the reconstructed output signal-to-noise ratio performance is provided in Section III. Theoretical performance bounds employing channel coding are described in Section IV. In particular, it is shown that these bounds indicate performance approaching the rate-distortion bound can be achieved with properly chosen error control protection. In Section V we demonstrate that these performance bounds are realistic in the sense that they can be approximated with a readily implemented class of convolutional codes. Simulation results are provided for typical real-world images in Section VI. Finally, in Section VII a summary and suggestions for future research are provided.

Paper approved by the Editor for Communication Theory of the IEEE Communications Society for publication after presentation at the 16th Annual Allerton Conference on Communications, Control, and Computing, Allerton, IL, October 1978. Manuscript received October 25, 1978; revised April 1, 1979. This work was supported in part by the Office of Naval Research under Contract N00014-75-C-0281.

The authors are with the Department of Electrical and Systems Engineering, Rensselaer Polytechnic Institute, Troy, NY 12181.

II. PRELIMINARIES

While there are a wide range of possible stochastic models for images, we will restrict attention to the class of 2-D autoregressive random fields described according to

$$S_{i,j} = \sum_{k=0}^{K} \sum_{l=0}^{L}{}' a_{k,l} S_{i-k,j-l} + W_{i,j}; \qquad i,j \geq 0 \tag{1}$$

where the prime is intended to indicate that the single point $k = l = 0$ is excluded from the double summation and $\{W_{i,j}\}$ is a 2-D zero-mean sequence of independent and identically distributed (i.i.d.) random variables possessing common variance σ_w^2. We assume that the initial values $S_{-k,-l}$ for $k = 0, 1, \cdots, K-1$ and $l = 0, 1, \cdots, L-1$ have been specified. These initial values represent the boundary terms as illustrated in Fig. 1.

As a concrete example of a 2-D autoregressive process we note the 2-D Gauss-Markov random field. Here

$$S_{i,j} = \rho_1 S_{i-1,j} + \rho_2 S_{i,j-1} - \rho_1 \rho_2 S_{i-1,j-1} + W_{i,j} \tag{2}$$

with $0 \leq |\rho_i| \leq 1$, $i = 1, 2$ and $\{W_{i,j}\}$ a 2-D i.i.d. zero-mean Gaussian sequence possessing common variance $\sigma_w^2 = \sigma_s^2 (1-\rho_1^2)(1-\rho_2^2)$. The quantity σ_s^2 represents the common variance of the resulting sequence $\{S_{i,j}\}$, i.e., $\sigma_s^2 = \text{var}\{S_{i,j}\}$, $i, j \geq 1$. It is implicitly assumed, of course, that the initial values $S_{0,0}$, $S_{k,0}$ and $S_{0,l}$ for $1 \leq k \leq K$ and $1 \leq l \leq L$ have been appropriately chosen to result in stationary conditions. We will use this 2-D Guass-Markov random field as an illustrative example in what follows.

0090-6778/79/1100-1644$00.75

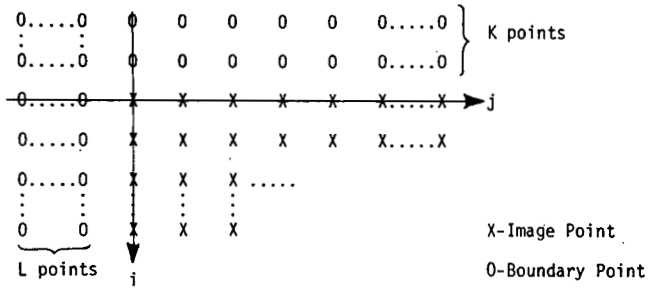

Figure 1 Illustration of Image and Boundary Points in 2-D Autoregressive Process.

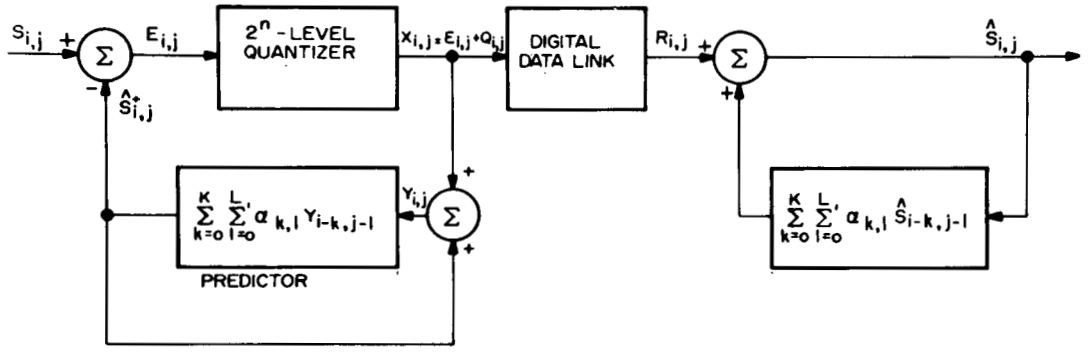

Figure 2 Block Diagram of Two-Dimensional DPCM Encoding/Decoding System.

An overall block diagram of the DPCM system under consideration is provided in Fig. 2. Following established nomenclature, the DPCM coding/decoding scheme is said to be matched to the message model if $\alpha_{i,j} = a_{i,j}$. That is, the coefficients in the feedback predictor are chosen equal to the 2-D autoregressive coefficients in (1). For analysis purposes we assume this to be the case although there may be good reason for other choices.

The notation of Fig. 2 deserves comment at this time. First the quantity

$$Y_{i,j} = S_{i,j} + Q_{i,j} \tag{3}$$

represents the *local estimate* of $S_{i,j}$ which is applied as input to the feedback predictor. In the absence of channel errors this is identical to $\hat{S}_{i,j}$ the *reproduced estimate* of $S_{i,j}$ released to the destination. The error incurred in this case is identical to the *instantaneous quantization error* $Q_{i,j}$. In the absence of quantization error and assuming $\alpha_{i,j} = a_{i,j}$, the quantity

$$\hat{S}_{i,j}^{+} = \sum_{k=0}^{K} \sum_{l=0}^{L}{}' \alpha_{k,l} Y_{i-k,j-l} \tag{4}$$

represents the *causal least mean-square predicted estimate* of $S_{i,j}$ making use of the data set as illustrated in Fig. 3. Note that in general due to the quantization errors inherent in $Y_{i,j}$, the quantity $\hat{S}_{i,j}^{+}$ will differ from the causal least mean-square predicted estimate of $S_{i,j}$. While it would be possible to use past† values of the sequence $\{S_{i,j}\}$ in making this prediction at the encoder, this information is unavailable at the decoder. In order to ensure that both the encoder and decoder utilize the same information and thus avoid an otherwise potentially unstable situation, the encoder will make use of $\{Y_{i,j}\}$ in forming the prediction $\hat{S}_{i,j}^{+}$.

† In this context "past" values represent elements in the data set used for causal prediction as illustrated in Fig. 3.

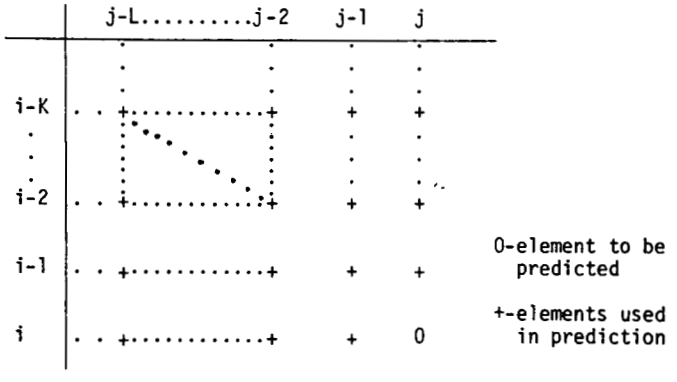

Figure 3 Illustration of Data Set Used in Causal Prediction of $S_{i,j}$.

In Fig. 2, the sequence $\{X_{i,j}\}$ represents the transmitted 2-D sequence whose values assume one of the $Q = 2^n$ possible output levels of the n-bit quantizer. Exclusive use will be made of a symmetric uniform quantizer. In particular, if Δ represents the uniform step size normalized to the standard deviation σ_e of the input error sequence $\{E_{i,j}\}$ then the input bin boundaries $\{E_l\}$ and output levels $\{X_l\}$ satisfy

$$E_l - E_{l-1} = X_l - X_{l-1} = \Delta\sigma_e; \qquad l = 0, 1, \cdots, Q \tag{5}$$

with the understanding $E_0 = -\infty$ while $E_Q = \infty$. The quantizer

output level $X_l = [l - (Q-1)/2]\Delta\sigma_e$, $l = 0, 1, \cdots, Q-1$ is then expressed as an n-bit binary word for subsequent transmission over the digital data link. In what follows we assume that a natural binary representation is employed. That is, the output level X_l is coded into the natural binary representation of the integer l. It will be assumed that individual bit streams are available for subsequent modulation/coding and transmission. In particular, the modulation/coding is allowed to be different for each of the n serial bit streams associated with the output of the n-bit quantizer.

In all cases, the quantizer characteristics are chosen to minimize the mean-square quantization error. That is, the single parameter Δ is chosen to minimize the quantity

$$\sigma_q^2 = E\{Q_{i,j}^2\} = \sum_{l=0}^{Q-1} \int_{E_l}^{E_{l+1}} [\xi - X_l]^2 p_E(\xi)\, d\xi \qquad (6)$$

where $p_E(\cdot)$ is the probability density function (p.d.f.) associated with the error sequence $\{E_{i,j}\}$. It is extremely difficult to provide explicit evaluation of $p_E(\cdot)$ in any realistic situation. As a result, we restrict attention to the two cases where the sequence $\{E_{i,j}\}$ is assumed either Gaussian or Laplacian distributed. From the experimental results provided in [6] there is substantial evidence that the error sequence $\{E_{i,j}\}$ is approximately Laplacian distributed for a wide-range of real-world images. For the 2-D Gauss-Markov random field described by (2), on the other hand, we would expect the error sequence to be approximately Gaussian distributed. The two cases considered then span a range of both practical and theoretical interest.

Tabulations of the optimum Δ for various numbers of quantization levels Q have been provided for the Gaussian distribution in Max [7], and likewise, for the Laplacian distribution in Paez and Glisson [8]. For convenience these results are summarized in Table 1. It should be noted, however, that the design approach employed here of optimizing the quantizer characteristics to minimize σ_q^2 is a decidedly suboptimum approach. That is, the quantizer characteristics should be chosen to minimize the overall reconstruction error. The mathematical intractability of the latter approach has influenced the approach adopted here.

Finally, the sequence $\{R_{i,j}\}$ appearing at the channel output is described according to

$$R_{i,j} = X_{i,j} + N_{i,j} \qquad (7)$$

where the sequence $\{N_{i,j}\}$ represents additive digital channel noise assumed independent from pixel-to-pixel. The reproducing estimate $\{\hat{S}_{i,j}\}$ delivered to the destination is then determined recursively according to

$$\hat{S}_{i,j} = \sum_{k=0}^{K} \sum_{l=0}^{L}{}' \alpha_{k,l} \hat{S}_{i-k,j-l} + R_{i,j}; \qquad i,j \geq 0 \qquad (8)$$

again assuming that appropriate initial conditions have been specified for $\hat{S}_{-k,-l}$ for $k = 0, 1, \cdots, K-1$ and $l = 0, 1, \cdots, L-1$. As noted previously, in the absence of channel errors

TABLE 1
SUMMARY OF NORMALIZED STEP SIZE Δ FOR OPTIMUM UNIFORM QUANTIZERS FOR BOTH GAUSSIAN AND LAPLACIAN ERROR SEQUENCES

Number of Output Levels Q	Normalized Step Size Δ	
	Gaussian	Laplacian
2	1.596	1.414
4	0.996	1.087
8	0.586	0.731
16	0.335	0.456
32	0.1881	0.281

(i.e., $R_{i,j} = X_{i,j}$) we have

$$\hat{S}_{i,j} = S_{i,j} + Q_{i,j} \qquad (9)$$

so that the only source of error is the quantization noise. The indexing of the channel output sequence $\{R_{i,j}\}$ must, of course, correspond to some established scanning pattern. In what follows we assume that the image is scanned in a fixed row-by-row raster scanning pattern and the sequence $\{R_{i,j}\}$ and hence $\{\hat{S}_{i,j}\}$ is ordered accordingly.

In Figs. 4 and 5 we illustrate typical behavior of this 2-D DPCM encoding scheme on a typical outdoor scene for an optimum uniform Gaussian and Laplacian quantizer respectively, both in the absence of channel errors. The images here, as in the remainder of the paper, are all 256 × 256 arrays. These results assume a first-order 2-D autoregressive image model similar to that described by (2). In particular, the order of the predictor $\hat{S}_{i,j}^+$ in (4) is such that $K = L = 1$. Least-squares estimates of the vertical and horizontal correlation coefficients, ρ_1 and ρ_2 respectively, were obtained and the predictor feedback coefficients set equal to the corresponding estimated quantities. The resulting estimates for the outdoor scene are $\rho_1 = 0.957$ and $\rho_2 = 0.967$. These values are typical for a wide range of real-world images.

In the absence of channel errors the 2-D DPCM encoding scheme provides reasonably good fidelity even for 1 bit/pixel although there are some distortions, particularly in the vicinity of sharp edges. There is marginal subjective improvement beyond 2-3 bits/pixel. Results using the Laplacian quantizer provide barely perceptible subjective improvement indicating some insensitivity to quantizer choice. In what follows, all displayed images will be for the case of an optimum uniform Laplacian quantizer unless explicitly noted to the contrary.

The effects of channel errors on the outdoor scene can be observed in Fig. 6. Here the channel is modeled as a binary symmetric channel (BSC) with bit error probability $P_b = 10^{-3}$. Subjective tests have indicated a sharp threshold at this point with reconstructed image quality degrading rapidly beyond this point. This is indicated most clearly in Figs. 7 and 8 indicating results for the outdoor scene at $P_b = 10^{-4}$ and $P_b = 5 \times 10^{-3}$ respectively. The effects of channel errors are much more pronounced as the number of quantization levels Q increases. Indeed, for these channel error rates it would ap-

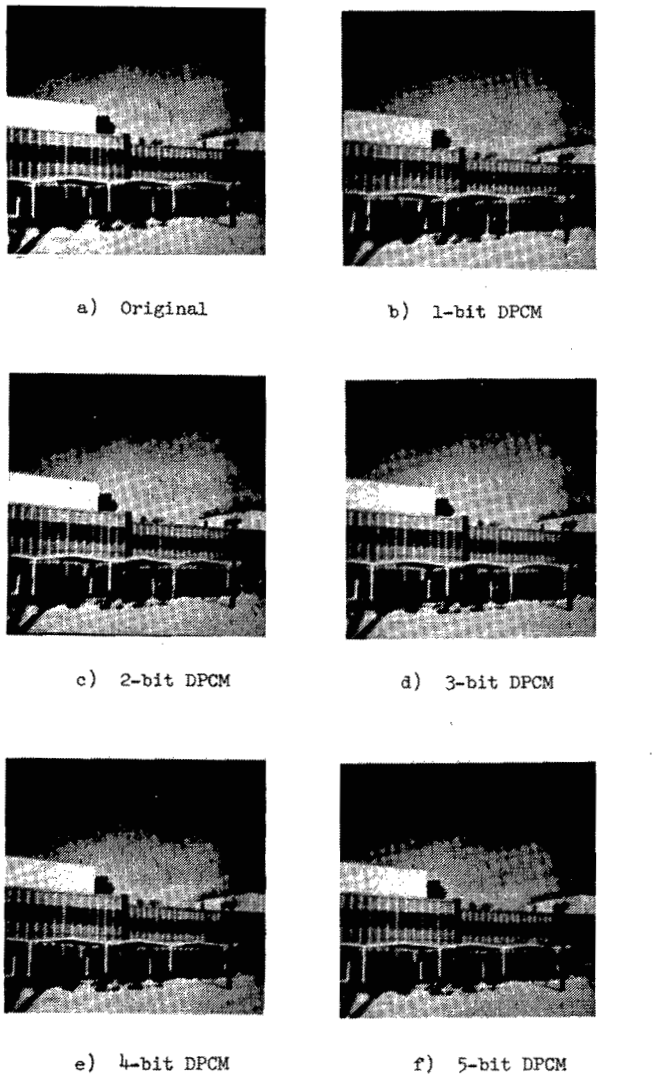

Figure 4 2-D DPCM Encoding of Typical Outdoor Scene. Quantization Effects on Reconstructed Image; Gaussian Quantizer.

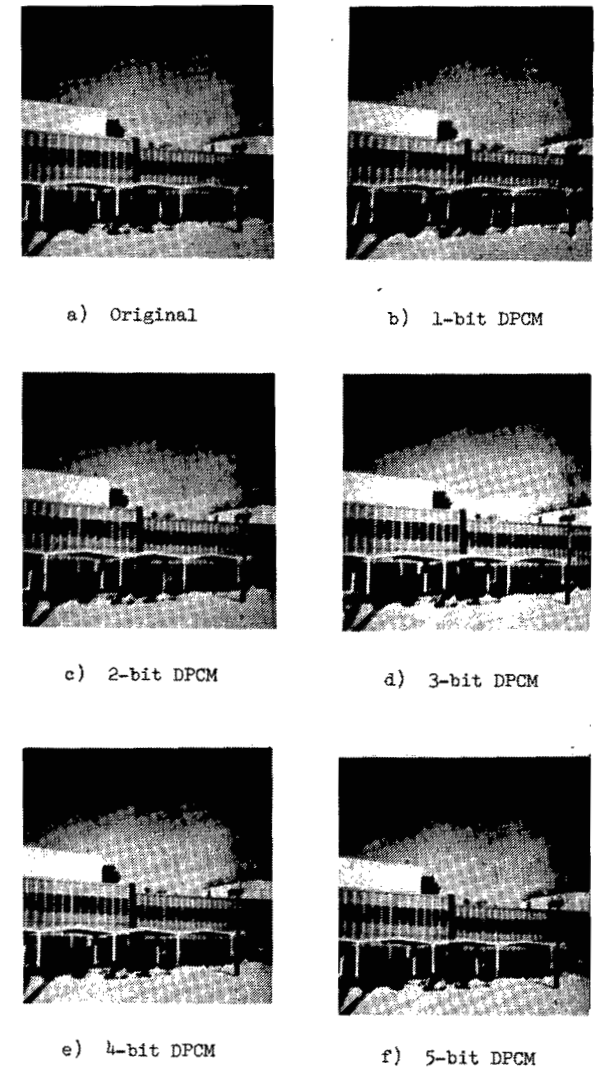

Figure 5 2-D DPCM Encoding of Typical Outdoor Scene. Quantization Effects on Reconstructed Image; Laplacian Quantizer.

pear wasteful of channel bandwidth to employ more than 1-2 bits/pixel. Increasing the quantizer accuracy degrades rather than improves image quality. Similar results apply in the case of a Gaussian quantizer. The explanation for this behavior can be seen most clearly from the explicit evaluation of output signal-to-noise ratio provided in the following section. We demonstrate how, by a judicious use of channel coding, the subjective image quality can be improved substantially in the presence of channel noise without sacrificing channel bandwidth.

III. ANALYSIS OF OUTPUT SIGNAL-TO-NOISE RATIO

The output signal-to-noise ratio (SNR_o) of the 2-D DPCM system is given by

$$\mathrm{SNR}_o = \frac{(\sigma_s^2/\sigma_e^2)}{e_T^2} \tag{10}$$

where σ_s^2 is the variance of the assumed zero-mean stationary 2-D sequence $\{S_{i,j}\}$ and

$$e_T^2 = E\{[S_{i,j} - \hat{S}_{i,j}]^2\}/\sigma_e^2 \tag{11}$$

is the resulting mean-square reconstruction error normalized to the variance σ_e^2 of the stationary sequence $\{E_{i,j}\}$ appearing as input to the quantizer. The quantity (σ_s^2/σ_e^2) has an interpretation as the mean-square signal level normalized to the mean-square prediction error which, if we neglect the effects of quantization noise, is easily shown to be given by

$$(\sigma_s^2/\sigma_e^2) = \left(\frac{1}{2\pi}\right)^2 \int_{-\pi}^{\pi} \int_{-\pi}^{\pi} |D(e^{j\lambda 1}, e^{j\lambda 2})|^2 \, d\lambda_1 \, d\lambda_2. \tag{12}$$

Here $D(z_1, z_2)$ is defined as a function of the complex variables z_1, z_2 as

$$D(z_1, z_2) = \frac{1}{1 - H(z_1, z_2)} \tag{13}$$

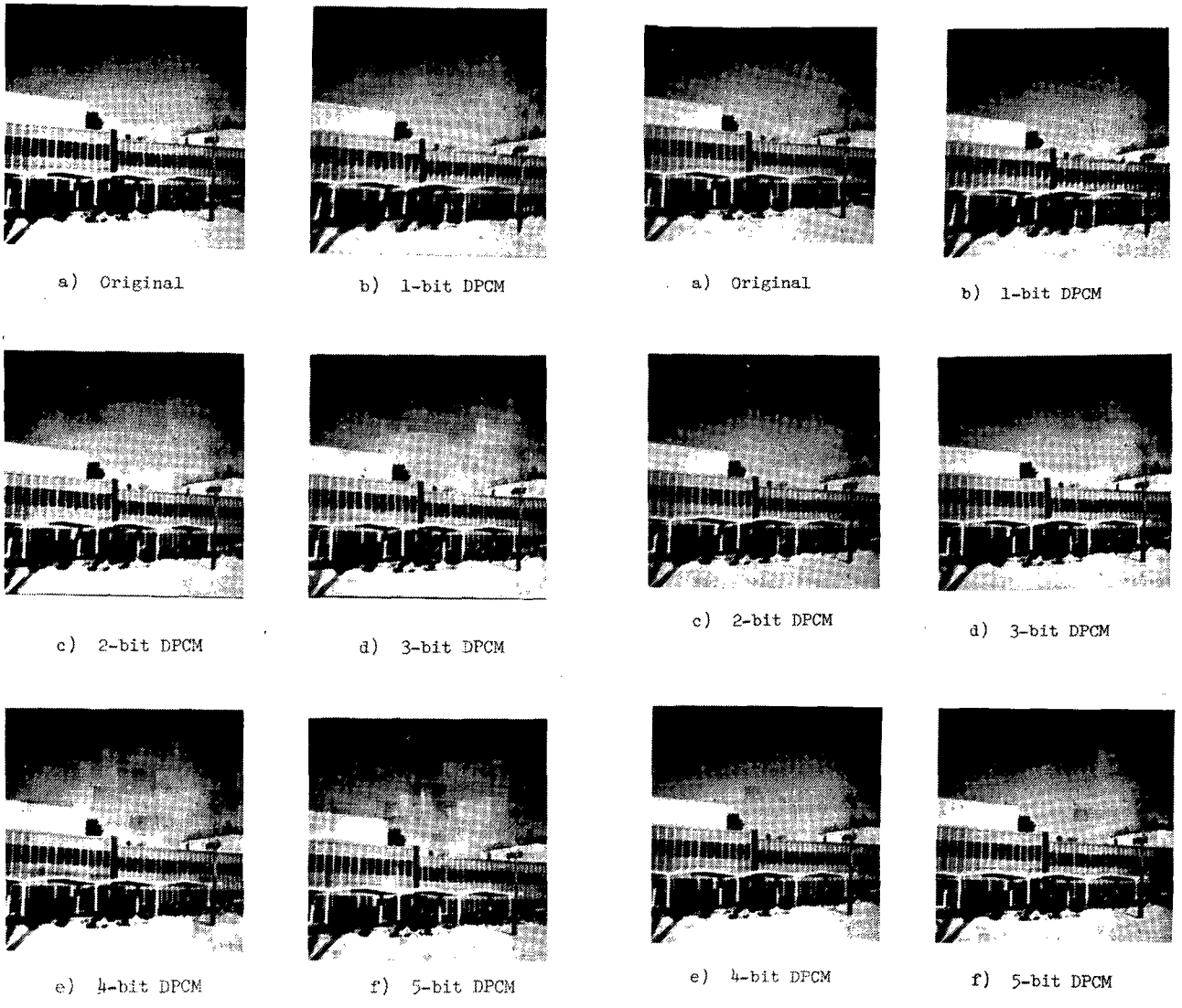

Figure 6 Channel Error Effects on 2-D DPCM Image Decoding. Typical Outdoor Scene; $P_b = 10^{-3}$.

Figure 7 Channel Error Effects on 2-D DPCM Image Decoding. Typical Outdoor Scene: $P_b = 10^{-4}$.

where $H(z_1, z_2)$ is the transfer function of the feedback predictor in the encoder. From (4) this quantity is given by

$$H(z_1, z_2) = \sum_{k=0}^{K} \sum_{l=0}^{L}{}' \alpha_{k,l} z_1^{-k} z_2^{-l}. \tag{14}$$

For example, in the case of the 2-D Gauss-Markov process in (2) we have

$$\sigma_s^2/\sigma_e^2 = \frac{1}{(1-\rho_1^2)(1-\rho_2^2)}. \tag{15}$$

Following a fairly standard development [9]-[12], the quantity e_T^2 in (10) can be expressed as the sum of three separate and conveniently normalized components according to

$$e_T^2 = \epsilon_q + 2\epsilon_m + \epsilon_c. \tag{16}$$

Here,

$$\epsilon_q = E\{Q_{i,j}^2\}/\sigma_e^2 = \sigma_q^2/\sigma_e^2$$

represents the mean-square value of the quantization noise normalized to σ_e^2. Similarly, the quantity ϵ_c represents the normalized mean-square error contribution due solely to channel errors and evaluated according to

$$\epsilon_c = E\{N_{i,j}'^2\}/\sigma_e^2 \tag{18}$$

where the stationary sequence $\{N_{i,j}'\}$ represents the additive noise at the output of the DPCM decoder in response to the channel noise sequence $\{N_{i,j}\}$ at its input. The system transfer function of the decoder $D(z_1, z_2)$ has been given previously by (13). Finally, the quantity ϵ_m represents a mutual error term given by

$$\epsilon_m = E\{Q_{i,j} N_{i,j}'\}/\sigma_e^2. \tag{19}$$

We consider evaluation of each of these terms separately.

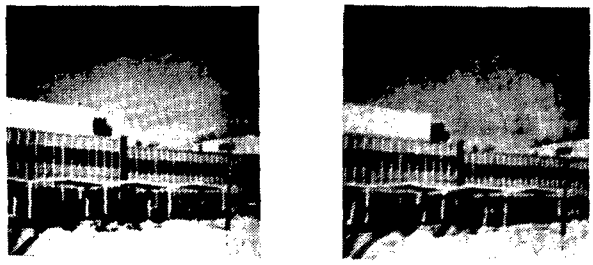

a) Original

b) 1-bit DPCM

c) 2-bit DPCM

d) 3-bit DPCM

e) 4-bit DPCM

f) 5-bit DPCM

Figure 8 Channel Error Effects on 2-D DPCM Image Decoding. Typical Outdoor Scene; $P_b = 5 \times 10^{-3}$.

As stated previously, the quantizer has been designed to minimize the variance σ_q^2 of the quantization noise. It is easily shown that

$$\epsilon_q = 2 \sum_{l=1}^{Q/2-1} \int_{(l-1)\Delta}^{l\Delta} [y - (l - 1/2)\Delta]^2 \hat{p}_E(y)\, dy + 2 \cdot \int_{(Q/2-1)\Delta}^{\infty} [y - (Q-1)\Delta/2]^2 \hat{p}_E(y)\, dy \tag{20}$$

where $\hat{p}_E(y) \triangleq \sigma_e p_E(\sigma_e y)$ is a normalized version of either the Gaussian or Laplacian p.d.f. possessing zero mean and unit variance. This expression for ϵ_q is easily evaluated numerically for various values of Q with Δ taken from Table 1.

Consider now the error term ϵ_c contributed by channel error effects as defined by (18). Assuming again that the channel noise sequence $\{N_{i,j}\}$ is independent from pixel-to-pixel with mean-square value e_n^2 we have

$$\epsilon_c = (e_n^2/\sigma_e^2)\left(\frac{1}{2\pi}\right)^2 \int_{-\pi}^{\pi} \int_{-\pi}^{\pi} |D(e^{j\lambda_1}, e^{j\lambda_2})|^2\, d\lambda_1\, d\lambda_2 \tag{21}$$

where $D(z_1, z_2)$ is the discrete 2-D system transfer function associated with the decoder and

$$e_n^2 = E\{N_{i,j}^2\} = \sum_{k=0}^{Q-1} \sum_{l=0}^{Q-1} (X_k - X_l)^2 P_{k|l} P_l. \tag{22}$$

This is merely the mean-square error incurred if X_l was transmitted and decoded as the level X_k averaged over the probability of all such error events. The quantity $P_{k|l}$ is the conditional probability that level X_l was transmitted and decoded as level X_k while P_l is the probability of transmitting level X_l. It is more illuminating to consider the normalized quantity e_n^2/σ_e^2 which is easily seen to reduce to

$$e_n^2/\sigma_e^2 = \Delta^2 \sum_{k=0}^{Q-1} \sum_{l=0}^{Q-1} (k-l)^2 P_{k|l} P_l. \tag{23}$$

In Appendix A it is shown that this last quantity can be evaluated according to

$$e_n^2/\sigma_e^2 = \Delta^2 \left\{ \sum_{i=0}^{n-1} P_{b_i}(1 - P_{b_i}) 2^{2i} \cdot \sum_{l=0}^{Q-1} + \left[\sum_{i=0}^{n-1} P_{b_i}(1 - 2l_i) 2^i \right]^2 p_l \right\} \tag{24}$$

Here l_i, $i = 0, 1, \cdots, n-1$ represent coefficients of the binary expansion of the integer l according to

$$l = \sum_{i=0}^{n-1} l_i 2^i; l_i = 0, 1, \tag{25}$$

while P_{b_i} is the bit error probability associated with the transmission of the i'th bit in the n-bit quantizer output word. For the particular case of equal bit error probability $P_{b_i} = P_b$, $i = 0, 1, \cdots, n-1$ this last expression reduces to

$$e_n^2/\sigma_e^2 = \Delta^2 P_b(1 - P_b)\{(Q^2 - 1)/3 + P_b \sum_{l=0}^{Q-1} [(Q-1) - 2l]^2 p_l\} \tag{26}$$

where we recall $Q = 2^n$. In either case, the error contribution ϵ_c is readily evaluated for various values of Q with Δ chosen from Table 1 for either the Gaussian or Laplacian quantizer characteristic. Again in the particular case of the 2-D Gauss-

Markov process given by (2) we find

$$\epsilon_c = \frac{e_n^2/\sigma_e^2}{(1-\rho_1^2)(1-\rho_2^2)} \tag{27}$$

with e_n^2/σ_e^2 given by either (24) or (26) as appropriate.

Finally, the mutual error term ϵ_m is shown in Appendix B to be expressible in the form

$$\epsilon_m = 2\Delta\left[\sum_{l=Q/2}^{Q-1}\left\{\sum_{i=0}^{n-1}(1-2l_i)P_{b_i}2^i\right\}\epsilon_l'\right]\left(\frac{1}{2\pi}\right)^2 \cdot \int_{-\pi}^{\pi}\int_{-\pi}^{\pi} D(e^{j\lambda_1}, e^{j\lambda_2})\,d\lambda_1\,d\lambda_2 \tag{28}$$

where

$$\epsilon_l' = \int_{E_l/\sigma_e}^{E_{l+1}/\sigma_e}\{y-[l-(Q-1)/2]\Delta\}\hat{p}_E(y)\,dy; \qquad l=0, 1, \cdots, Q-1 \tag{29}$$

is the average normalized quantization error given that the l'th level was transmitted. For the particular case where the bit error probability is constant for each bit position we have

$$\epsilon_m = -4\Delta P_b\left[\sum_{l=Q/2}^{Q-1}\{l-(Q-1)/2\}\epsilon_l'\right]\left(\frac{1}{2\pi}\right)^2 \cdot \int_{-\pi}^{\pi}\int_{-\pi}^{\pi} D(e^{j\lambda_1}, e^{j\lambda_2})\,d\lambda_1\,d\lambda_2. \tag{30}$$

In either case, the quantity ϵ_m is readily computed as a function of Q and the channel error probability for various image models.

For the particular case of the 2-D Gauss-Markov sequence described by (2) it is readily seen that

$$\left(\frac{1}{2\pi}\right)^2\int_{-\pi}^{\pi}\int_{-\pi}^{\pi} D(e^{j\lambda_1}, e^{j\lambda_2})\,d\lambda_1\,d\lambda_2 = 1 \tag{31}$$

which simplifies evaluation of ϵ_m. This component has been found to be negligible compared to the other error components ϵ_q and ϵ_c.

In Fig. 9 we illustrate the behavior of SNR_o for an assumed 2-D Gauss-Markov image model of the outdoor scene. Results for a much wider range of real-world images are similar. Here a Gaussian uniform quantizer was used and individual bits were transmitted using coherent binary phase-shift keyed (BPSK) modulation over an additive white Gaussian noise (AWGN) channel. The bit error probability in this case is given by

$$P_{b_i} = Q\left(\sqrt{\frac{2E_{si}}{N_0}}\right); \qquad i=0, 1, \cdots, n-1 \tag{32}$$

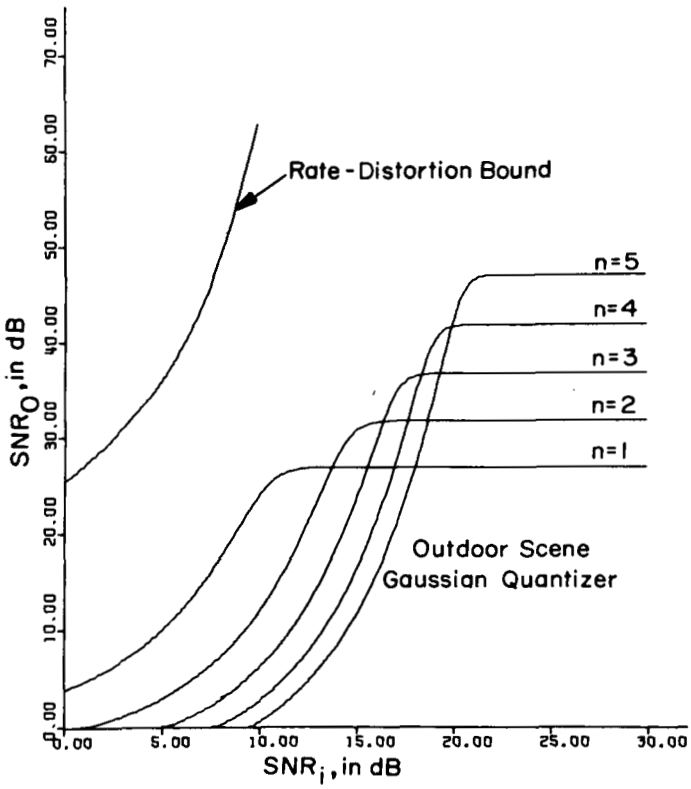

Figure 9 Uncoded 2-D DPCM System Performance for Outdoor Scene; Gaussian Quantizer.

where

$$Q(x) \triangleq \frac{1}{\sqrt{2\pi}}\int_x^{\infty} e^{-y^2/2}\,dy \tag{33}$$

and E_{si} is the signal energy per transmitted binary channel symbol while $N_0/2$ is the double-sided noise spectral density in watts/Hz.

In these figures, the quantity SNR_o is plotted as a function of the channel signal-to-noise ratio on a normalized per pixel basis. That is, if N_c uses of the channel are employed to transmit the n-bit quantizer output word corresponding to each pixel position then the channel input signal-to-noise ratio is defined according to

$$\mathrm{SNR}_i = \sum_{i=0}^{N_c-1}(2E_{si}/N_0) \tag{34}$$

where E_{si}, $i = 0, 1, \cdots, N_c - 1$ is the signal energy for each channel use. Actually, in Fig. 9, $N_c = n$ while we assume constant energy so that $E_{si} = E_s$, $i = 0, 1, \cdots, n-1$. It will prove convenient when employing channel coding to allow the generality afforded by (34). The bandwidth expansion factor is then N_c/n.

Also included in Fig. 9 is the rate-distortion bound on SNR_o for operation over an AWGN channel. Following the technique described by Goblick [13] and Goblick and Holsinger [14], this is obtained by equating the rate-distortion

function, computed under a mean-square fidelity criterion, to the channel capacity and solving for SNR_o as a function of SNR_i. The rate-distortion function for a continuous-amplitude 2-D Gaussian sequence has been given by Stuller and Kurz [15] following the development by Berger [16] in the 1-D case. In particular, the rate-distortion function $R(D)$ has the parametric form

$$D = \left(\frac{1}{2\pi}\right)^2 \int_{-\pi}^{\pi}\int_{-\pi}^{\pi} \min\{\theta, S(\lambda_1,\lambda_2)\}\, d\lambda_1\, d\lambda_2 \qquad (35a)$$

and

$$R(D) = \left(\frac{1}{2\pi}\right)^2 \int_{-\pi}^{\pi}\int_{-\pi}^{\pi} \max\left\{0, \tfrac{1}{2}\log_2 \frac{S(\lambda_1,\lambda_2)}{\theta}\right\} d\lambda_1\, d\lambda_2 \qquad (35b)$$

measured in units of bits/sample. Here $S(\lambda_1, \lambda_2)$ represents the 2-D discrete power spectral density which for a 2-D autoregressive process as in (1) becomes

$$S(\lambda_1,\lambda_2) = \left| \frac{1}{1 - \sum_{k=0}^{K}{\sum_{l=0}^{L}}' a_{k,l} e^{-jk\lambda_1} e^{-jl\lambda_2}} \right|^2. \qquad (36)$$

In the particular case of the 2-D Gauss-Markov process this reduces to

$$S(\lambda_1,\lambda_2) = \frac{(1-\rho_1{}^2)(1-\rho_2{}^2)\sigma_s{}^2}{(1-2\rho_1\cos\lambda_1+\rho_1{}^2)(1-2\rho_2\cos\lambda_2+\rho_2{}^2)}. \qquad (37)$$

A computer program for the numerical evaluation of $R(D)$ has been constructed as described in [17]. In the present context, we have $SNR_o = \sigma_s{}^2/D$ where D is the mean square distortion.

The capacity of the AWGN channel with signal energy E_{si} is given by the well-known expression [18]

$$C = \tfrac{1}{2}\log_2\left[1 + \frac{2E_{si}}{N_0}\right] \text{(bits/channel use)} \qquad (38)$$

so that the maximum output SNR for N_c channel uses satisfies††

$$R(\sigma_s{}^2\, SNR_o{}^{-1}) = \frac{N_c}{2}\log_2\left[1 + \frac{SNR_i}{N_c}\right] \qquad (39)$$

allowing solution for SNR_o in terms of SNR_i.

Several things should be observed from Fig. 9. In the first place, note the sharp threshold which becomes more pronounced as the number of quantization levels Q increases. For SNR_i in excess of approximately 20 dB channel errors are rare and the performance is limited solely by quantization noise. An increase in the number of quantization levels results in a commensurate increase in SNR_o. For smaller SNR_i we see a complete reversal of this behavior. For example, at SNR_i = 12 dB relative performance, measured in terms of SNR_o, actually improves by decreasing the number of quantization levels. This is an illustration of the behavior observed previously in Figs. 6 through 8. It should be noted that this threshold behavior occurs at error probabilities typical of that provided on many commercial and military data links.

The second observation to be made from Fig. 9 is that this 2-D DPCM scheme is relatively inefficient compared to the rate-distortion bound. In the next section we develop ultimate performance bounds to be achieved through channel coding. These bounds are based upon information-theoretic considerations and apply to all classes of codes. Results indicate relative performance arbitrarily close to the rate-distortion bound over a useful range of SNR_i. Later we demonstrate that these performance bounds are realistic in the sense that they can be closely approximated with an easily implemented class of convolutional codes.

IV. THEORETICAL PERFORMANCE BOUNDS

A useful *upper* bound on SNR_o can be obtained by *lower* bounding the bit error probability P_{b_i}, $i = 1, 2, \cdots, n-1$ associated with each of the bits in the n-bit quantizer output word. Consider first the case where the modulation/coding system treats each bit identically. Recall that N_c uses of the channel are required to transmit the quantizer output word so that the normalized code rate in bits per channel use is $R = n/N_c$. Under the AWGN assumption, the channel capacity is given by (38) with $E_{si} = E_s$, the constant energy per channel use. The converse to the coding theorem (cf. [18], [19]) then provides the desired lower bound on the common bit error probability P_b. Following the particularly illuminating development in McEliece [20], at rates above the capacity C of the AWGN channel, the bit error probability achievable by any rate R code is bounded away from zero by

$$P_b \geq H^{-1}(1 - C/R) \qquad (40)$$

where $H^{-1}(\cdot)$ represents the inverse of the *binary entropy function*

$$H(x) = -x\log_2 x - (1-x)\log_2(1-x); \qquad 0 < x < 1. \qquad (41)$$

At rates below capacity P_b can be made negligibly small. For purposes of numerical evaluation, P_b will be computed according to the right-hand side of (40) for $R > C$ and we set $P_b = 0$ for $R \leq C$. It should be noted that this approach is similar to that employed by Chase et al. [21], who observe that no known codes can achieve this lower bound on P_b and even for $R < C$ infinitely long codes are required to achieve arbitrarily small bit error probability. Nevertheless, as we shall see, this bound does provide a useful perspective in assessing the efficacy of combined source-channel coding.

†† We assume constant signal energy so that $E_{si} = E_s$, $i = 0, 1, \cdots, N_c - 1$.

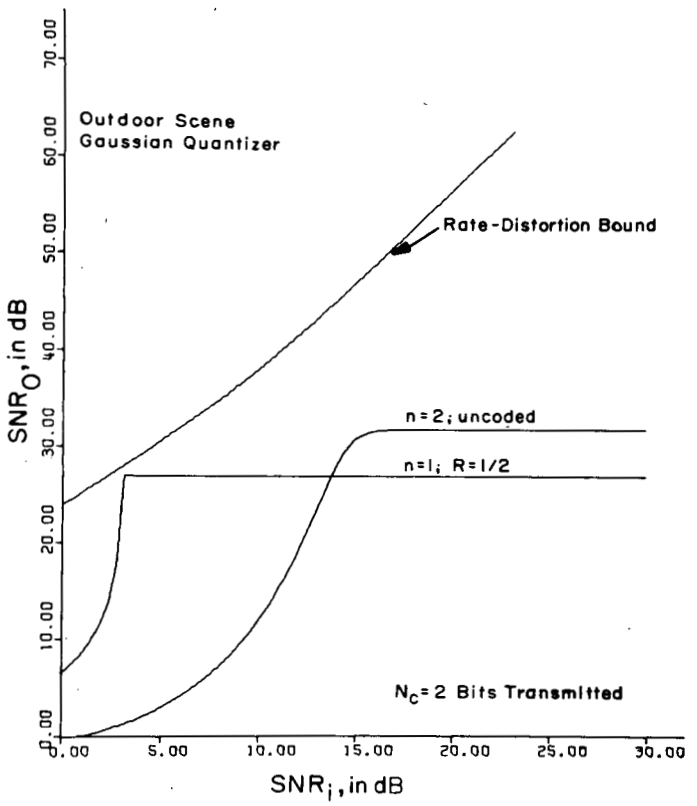

Figure 10 Performance Bounds for Optimum Fixed-Rate Codes; Outdoor Scene; Gaussian Quantizer.

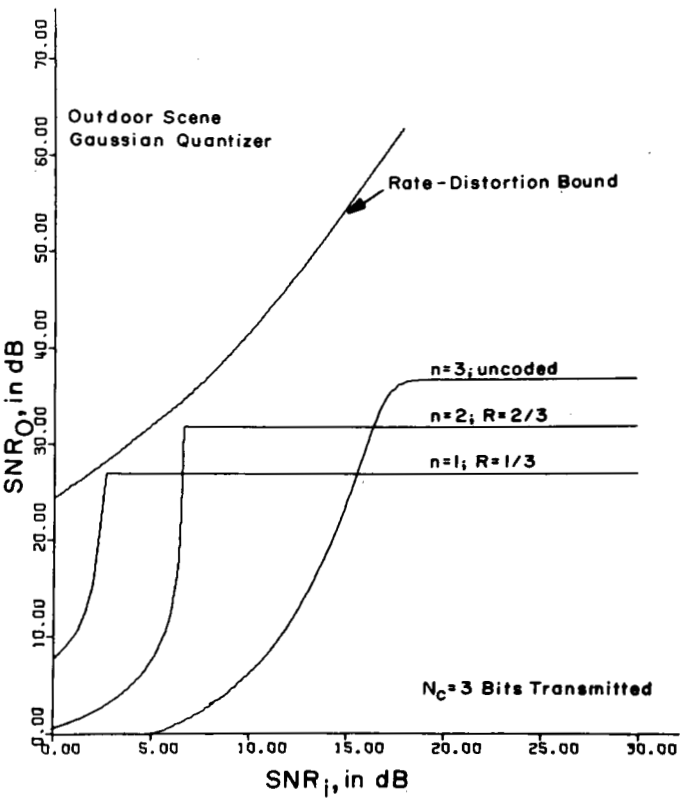

Figure 11 Performance Bounds for Optimum Fixed-Rate Codes; Outdoor Scene; Gaussian Quantizer.

In Figs. 10-12 we illustrate typical performance results for the outdoor scene employing a fixed-rate modulation/coding approach. Similar results hold for a much wider class of real-world images. In each of these figures, the total number of channel uses is held fixed at the values $N_c = 2, 3, 4$ respectively while the number of bits used in the quantizer assume the values $n = 1, 2, \cdots, N_c$. Fixed-rate $R = n/N_c$ codes then ensure common transmission bandwidth requirements associated with all curves on the same figure. These curves indicate clearly the nature of the tradeoffs possible between quantization accuracy and sensitivity to channel errors at a fixed transmission bandwidth. The coded system performance is characterized by a reduction in saturation level SNR_o but with a threshold occurring at significantly lower SNR_i. Indeed, the knee of this threshold characteristic occurs in all cases within 2-3 dB of the rate-distortion bound. For example, from Fig. 10 if $SNR_o \geqslant 25$ dB is required at SNR_i as low as 5 dB and allowing only two channel uses to transmit each pixel level a 1-bit quantizer is required in conjunction with a rate $R = 1/2$ code. This level of performance could not be achieved with a 2-bit quantizer and no coding.

While the fixed-rate coding approach appears to offer performance approaching the rate-distortion bound, it should be noted that codes of fairly unusual rates like $R = 2/3, 3/4, 4/5$, etc. are required. Relatively little is known concerning the construction and properties of practical codes of these rates. In Figs. 13 and 14 we illustrate performance bounds on SNR_o, again for the outdoor scene, when each bit in the quantizer output word can be accessed and separately coded. Attention

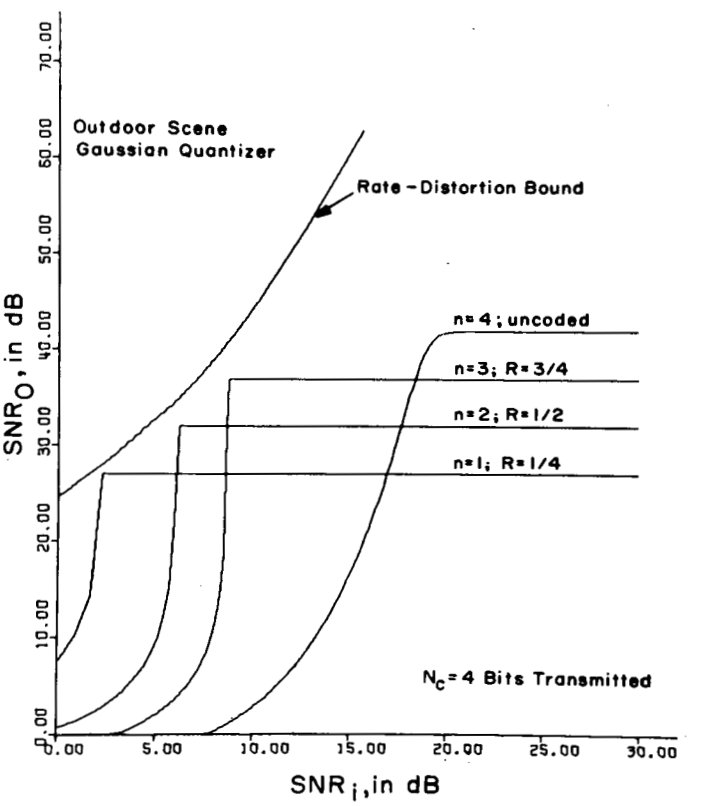

Figure 12 Performance Bounds for Optimum Fixed-Rate Codes; Outdoor Scene; Gaussian Quantizer.

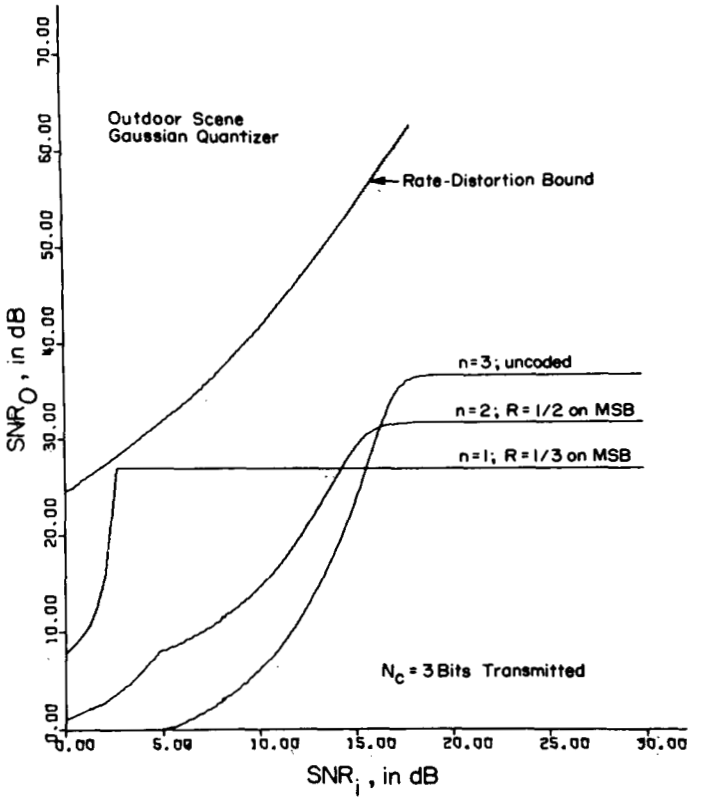

Figure 13 Performance Bounds for Optimum Practical-Rate Codes Combined with No Coding; Outdoor Scene; Gaussian Quantizer.

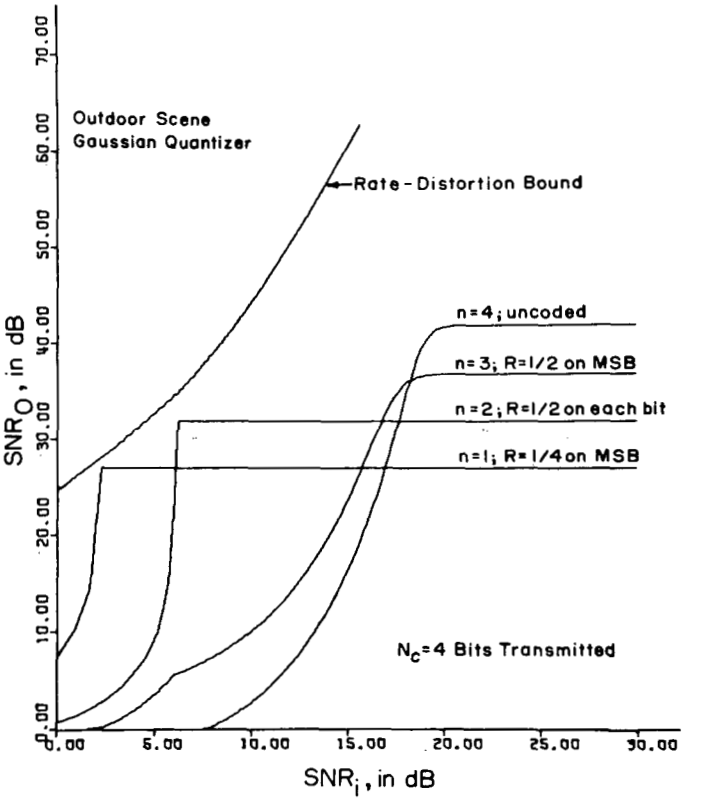

Figure 14 Performance Bounds for Optimum Practical-Rate Codes Combined with No Coding; Outdoor Scene; Gaussian Quantizer.

is restricted to code rates of $R = 1/2$, $1/3$, and $1/4$ since a variety of practical codes exist at these rates. Again each of these figures corresponds to a fixed number of channel uses per pixel. Error control protection is applied only to the most significant bit(s) (MSB) since errors here contribute most heavily to reconstructed image quality. For example, in Fig. 13 the number of channel uses per pixel is fixed at $N_c = 3$. The several tradeoffs include a 3-bit uncoded system, a 2-bit system with an $R = 1/2$ code on the MSB with the remaining bit unprotected, and finally a 1-bit system with an $R = 1/3$ code employed on the only bit. Examination of these figures indicates the relative weakness of this approach compared to the fixed rate systems. In particular, unless some degree of error protection is applied to *all* bits of the quantizer output word, the threshold continues to exist at uncomfortably large values of SNR_i and the performance is relatively poor compared to the rate-distortion bound. This behavior is due to the residual mean-square error contributions from unprotected bit errors.

V. PRACTICAL CHANNEL CODE PERFORMANCE

The advantages of fixed rate channel coding in conjunction with 2-D DPCM source coding have been illustrated in the preceding section. Restriction to practical code rates, however, generally resulted in unequal error protection to each of the bits associated with a quantizer output word. Nevertheless, this latter approach can be quite effective in recovering most of the performance gains associated with the fixed rate scheme. It remains to demonstrate the degree to which these ultimate performance bounds can be approached by practical coding schemes. In particular, we restrict attention to short constraint length convolutional codes of rates $R = 1/2$, $1/3$ and $1/4$ decoded using the Viterbi algorithm, an excellent description of which can be found in [22]. The optimum binary codes tabulated by Odenwalder [23] and Larsen [24] are used exclusively in what follows.

A useful exponentially tight bound on bit error probability obtained with Viterbi decoding on memoryless channels can be expressed in the general form

$$P_b \leq K_0 \left.\frac{dT(N,D)}{dN}\right|_{N=1,D=D_0} \tag{42}$$

where $T(D,N)$ is the code generating function (cf. [22] for details) while the constants K_0 and D_0 depend upon the particular code employed, the modulation strategy in use and the channel parameters. For example, for BPSK modulation on the AWGN channel we have

$$K_0 \triangleq Q\left(\sqrt{\frac{2d_f RE_b}{N_0}}\right)\exp\left\{\frac{d_f RE_b}{N_0}\right\} \tag{43a}$$

while

$$D_0 = \exp\left\{-\frac{RE_b}{N_0}\right\} \tag{43b}$$

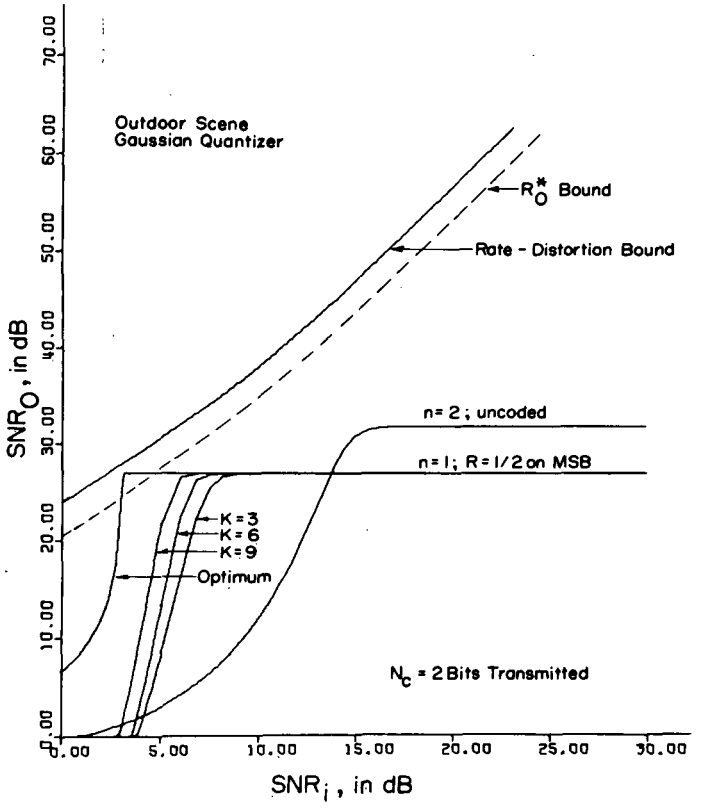

Figure 15 Practical Convolutional Code Performance; Outdoor Scene; Gaussian Quantizer.

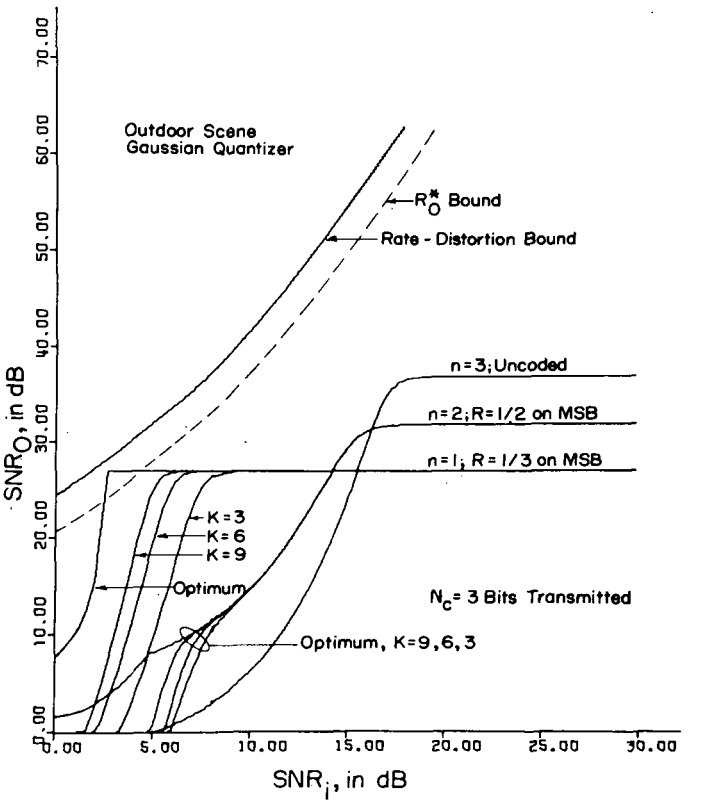

Figure 16 Practical Convolutional Code Performance; Outdoor Scene; Gaussian Quantizer.

where d_f is the free distance of the code, R is the normalized code rate in information bits transmitted per channel use and finally E_b/N_0 is the energy per information bit normalized to the single-sided noise spectral density N_0 watts/Hz. The quantity E_b is related to the energy per channel symbol E_s according to $E_s = RE_b$. A computer program has been developed [25] allowing numerical evaluation of this bound and thus explicit evaluation of SNR_o.

Typical results are illustrated in Fig. 15 for the case $N_c = 2$ channel uses per pixel where practical codes of constraint length $K = 3$, 6 and 9 have been employed. Similar results are provided in Fig. 16 for the case $N_c = 3$. These figures correspond to the optimum code results in Figs. 10 and 13 respectively. The convergence of the practical code performance toward the optimum performance with increasing constraint length K is illustrated clearly in Figs. 15 and 16. Unfortunately, the performance even for a $K = 9$ code falls short of the optimum code performance by some 2-3 dB and slightly more when compared to the rate-distortion bound.

Also included in Figs. 15 and 16 is a dotted curve labeled R_0* bound which is displaced some 2-3 dB from the rate distortion bound. We feel that this quantity provides a more realistic bound on achievable performance than the rate distortion bound. In particular, it is well-known (cf. [11], [26]) that there exists a *block* code of rate R and block length N such that the probability of error in decoding a source word of length $K = NR$ is bounded according to:

$$P_e \leq 2^{-N[R_0 - R]}; \qquad R < R_0 \tag{44}$$

where R_0 is the so-called critical rate associated with the modulator/channel/demodulator cascade. Thus, for block codes, the single number R_0 provides a measure of both a range of rates R for which reliable communication is possible as well as the coding complexity, as reflected by N, required to guarantee a specified block-error probability. More recently, Viterbi [27] has shown for convolutional coding and maximum-likelihood sequence decoding on the constant, discrete memoryless channel that the error probability is upper bounded according to

$$P_e \leq C_R L 2^{-K(R_0/R)} \qquad \text{if } R < R_0, \tag{45}$$

where K is the constraint length of the convolutional code, R is the code rate, L is the total number of source letters encoded, and C_R is a weakly dependent function of R and not a function of L and K. Thus, as with block codes, the single number R_0 provides a measure of both reliable rates and code complexity. Massey [28], [29] has used these observations to make an eloquent and persuasive argument for adopting R_0 as a modulator-demodulator design parameter in place of the more commonly used error probability.

As Wozencraft and Jacobs [26] demonstrate, the quantity

$$R_0^* = \frac{\log_2 e}{2}\left[1 + E_s/N_0 - \sqrt{1 + (E_s/N_0)^2}\right] + \tfrac{1}{2}\log_2\left[\tfrac{1}{2}\left(1 + \sqrt{1 + (E_s/N_0)^2}\right)\right] \tag{46}$$

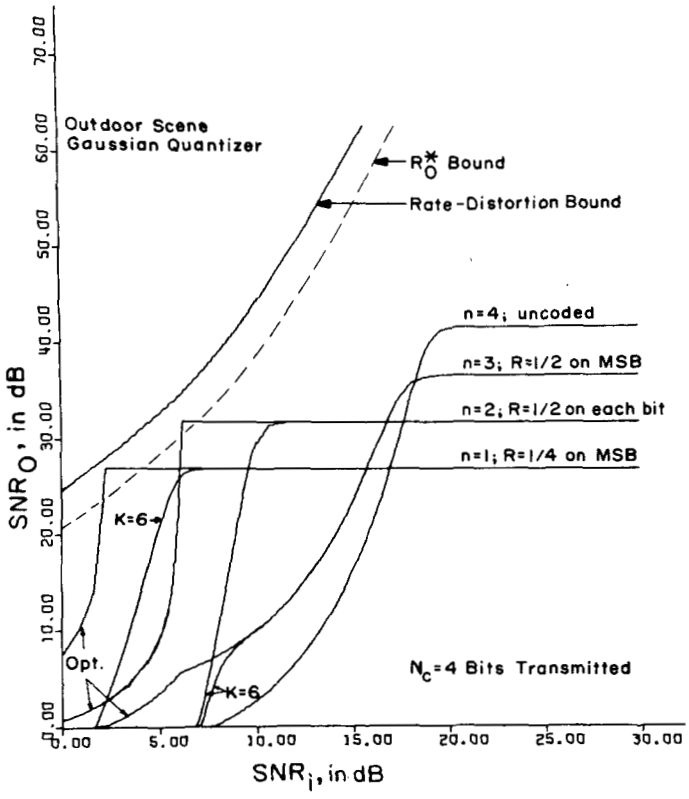

Figure 17 Practical Convolutional Code Performance; Outdoor Scene; Gaussian Quantizer.

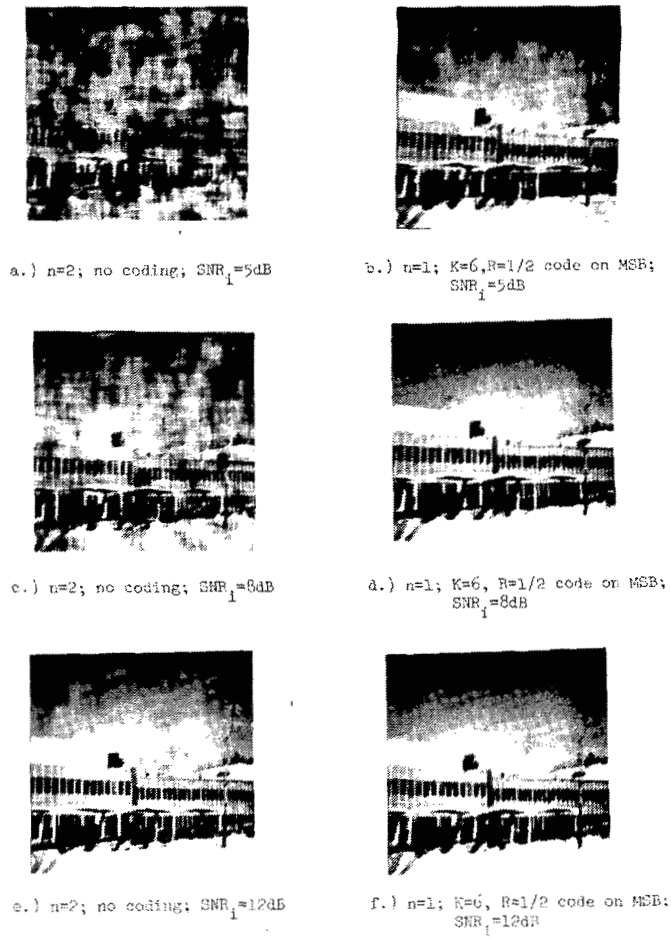

Figure 18 Simulation Results on Outdoor Scene; N_c = 2 Bits Transmitted.

provides a useful upper bound on R_0 on the AWGN channel for any choice of modulator-demodulator parameters. The parameter $R_0^* < C$ then provides a more realistic limit than the channel capacity C on the range of rates achievable on the AWGN channel. In Figs. 15 and 16 the curve labeled R_0^* bound then is obtained by equating R_0^* to the rate-distortion function $R(D)$ and solving for SNR_o as a function of SNR_i. We see then that the use of practically implemented short constraint length convolutional codes results in performance within 1-2 dB of the "practically achievable" R_0^* bound. Similar conclusions can be drawn from Fig. 17 corresponding to $N_c = 4$ channel uses. Here results are shown only for practical $K = 6$ codes.

VI. SIMULATION RESULTS

The effectiveness of the combined source-channel coding scheme employing selected constraint length $K = 6$ convolutional codes are illustrated in the case of the outdoor scene by the simulation results provided in Figs. 18-20 for $N_c = 2, 3$, and 4 respectively. Corresponding analytical performance evaluation is illustrated by the respective curves in Figs. 15-17. Similar results have been obtained with a variety of real-world images. In all these figures, SNR_i is constant across a row while the number of quantization bits n is held constant for each column. The transmission bandwidth requirements, as indicated by the number N_c of channel uses per pixel, is constant for all reconstructed images on a figure. Representative choices for SNR_i in each case were made just below and above pronounced thresholds in the SNR_o curves described in the preceding section.

These figures illustrate the dramatic improvements in subjective reconstructed image quality resulting from a judicious tradeoff between quantization accuracy and error control protection in a fixed transmission bandwidth. For example, in Fig. 20 we see clearly the advantages of allocating excess transmission bandwidth to error control rather than in attempting to improve the quantization accuracy by increasing the number of quantization levels. In this example, the 2-bit quantizer employing a $K = 6$, $R = 1/2$ code on each bit provides far superior reconstructed image quality than the 4-bit uncoded system or even the 3-bit system with error control protection on only the MSB.

VII. SUMMARY AND CONCLUSIONS

We have described an approach to the combined source-channel coding of a particular class of image sources. This approach offers theoretical performance approximating the rate distortion bound. We have shown how this theoretical performance can in turn be approximated by a class of practical short constraint length convolutional codes and we have demonstrated the performance gains through selected simulations on real-world images. The major deficiency lies in the lack of

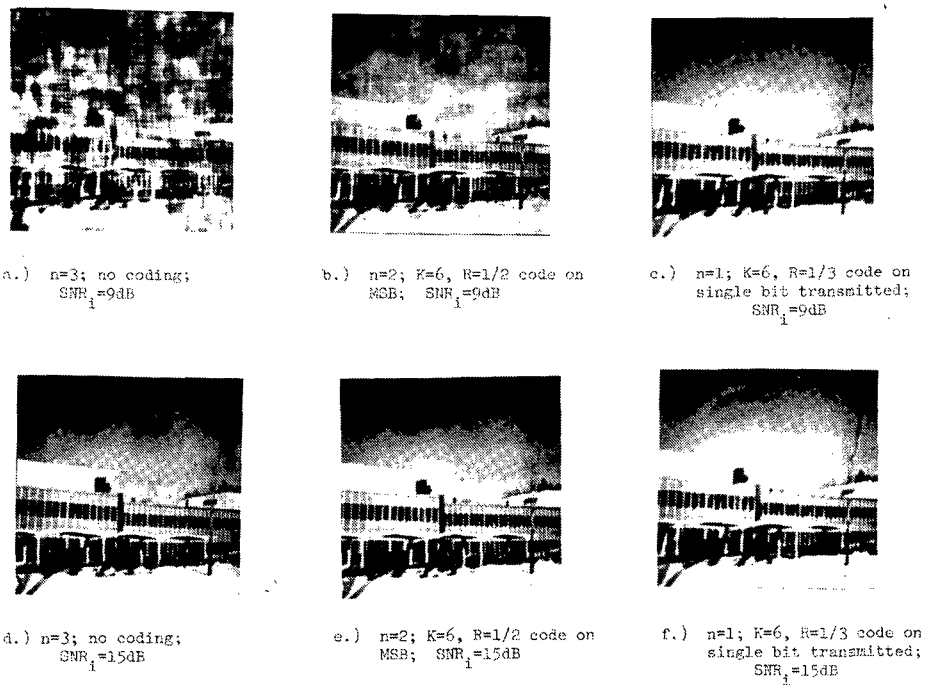

a.) n=3; no coding; SNR_i=9dB
b.) n=2; K=6, R=1/2 code on MSB; SNR_i=9dB
c.) n=1; K=6, R=1/3 code on single bit transmitted; SNR_i=9dB
d.) n=3; no coding; SNR_i=15dB
e.) n=2; K=6, R=1/2 code on MSB; SNR_i=15dB
f.) n=1; K=6, R=1/3 code on single bit transmitted; SNR_i=15dB

Figure 19 Simulation Results on Outdoor Scene; N_c = 3 Bits Transmitted.

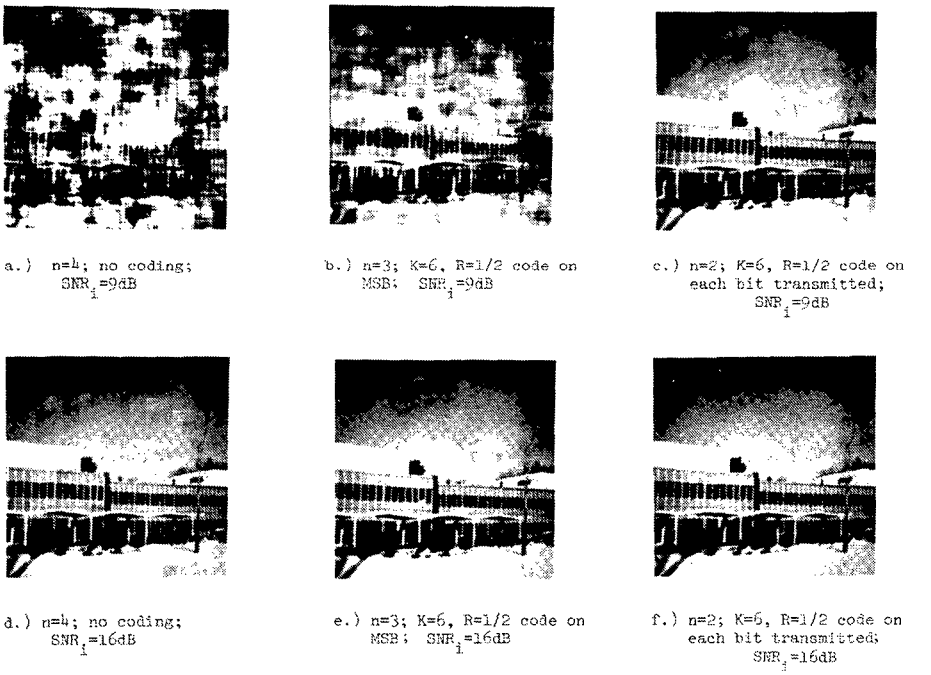

a.) n=4; no coding; SNR_i=9dB
b.) n=3; K=6, R=1/2 code on MSB; SNR_i=9dB
c.) n=2; K=6, R=1/2 code on each bit transmitted; SNR_i=9dB
d.) n=4; no coding; SNR_i=16dB
e.) n=3; K=6, R=1/2 code on MSB; SNR_i=16dB
f.) n=2; K=6, R=1/2 code on each bit transmitted; SNR_i=16dB

Figure 20 Simulation Results on Outdoor Scene; N_c = 4 Bits Transmitted.

good high rate code constructions required to achieve the near optimum behavior indicated by the fixed-rate code performance results. More specifically, we have been forced to utilize previously tabulated optimum codes for rates R = 1/2, 1/3 and 1/4. This severly compromises the flexibility of the approach in those situations where extremely high quality image reconstruction is required, i.e., high saturation level SNR_o at low SNR_i. For more moderate reconstruction image quality requirements this restriction to available codes does not present a problem as demonstrated, for example, by Fig. 17 and the corresponding simulation results in Fig. 20. The result then, at least for moderate reconstructed image quality requirements, is a relatively robust design which offers a near optimum compromise between quantization accuracy and sensitivity to channel errors while preserving a fixed transmission bandwidth requirement. Work is in progress to determine and tabulate the properties of good short constraint length convolutional codes operating at the relatively high rates of R =

3/5, 2/3, 3/4, etc. This should extend the flexibility of the approach considerably.

Another issue which deserves attention is the question of image modeling. We have assumed that the images of interest could be modeled as 2-D autoregressive models. Indeed, numerical results were provided only for the first-order 2-D Gauss-Markov model. The assumption of autoregressive behavior with Gaussian statistics is a gross oversimplification. Similar considerations apply, however, to more general stochastic image models and this aspect is presently under investigation.

Finally, it should be noted that we have made exclusive use of a uniform quantizer. This has certainly simplified the analysis but does raise the question of whether significant improvement can be realized through improved quantizer design. We feel that only marginal improvements can be expected by redesign of the quantizer although this question is being explored.

APPENDIX A

EVALUATION OF NORMALIZED MEAN-SQUARE ERROR DUE TO CHANNEL NOISE

The normalized mean-square error due solely to channel noise is given by Eqn. (23) of the text which is repeated below for convenience

$$e_n^2/\sigma_e^2 = \Delta^2 \sum_{k=0}^{Q-1} \sum_{l=0}^{Q-1} (k-l)^2 P_{k|l} P_l \tag{A-1}$$

where each of the terms has previously been defined. By interchanging the order of summation, the summation on k is easily evaluated. In particular, this summation is recognized as the conditional mean of quantity $(k-l)^2$ given that the level l was transmitted. That is,

$$E\{(k-l)^2 \mid l\} = \sum_{k=0}^{Q-1} (k-l)^2 P_{k|l} = \overline{k^2} - 2\bar{k}l + l^2 \tag{A-2}$$

where, for convenience, the overbar indicates conditional expectation given the level l was transmitted. We evaluate each of these terms separately. Consider first the quantity $\bar{k}$. The integer k can be expressed as

$$k = \sum_{i=0}^{n-1} k_i 2^i; \qquad k = 0, 1, \cdots, Q-1 \tag{A-3}$$

where $k_i = 0, 1$. Observe that

$$\bar{k} = \sum_{i=0}^{n-1} \bar{k}_i 2^i \tag{A-4}$$

while

$$\bar{k}_i = (1-P_{b_i})l_i + P_{b_i}(1-l_i); \qquad i = 0, 1, \cdots, n-1 \tag{A-5}$$

$$= (1-2P_{b_i})l_i + P_{b_i}$$

where $l_i = 0, 1$ is the corresponding element in the binary expansion of the integer l representing the transmitted signal level and P_{b_i} is the bit-error probability associated with the i'th bit which is allowed to be different for each bit position. It follows then that

$$\bar{k} = \sum_{i=0}^{n-1} \{(1-2P_{b_i})l_i + P_{b_i}\}2^i$$

$$= l + \sum_{i=0}^{n-1} (1-2l_i)P_{b_i}2^i. \tag{A-6}$$

This shows, in particular, that there is a bias introduced in the declaration of channel output level due to channel errors. In the particular case when the bit error probabilities are all equal so that $P_{b_i} = P_b, i = 0, 1, \cdots, n-1$, we have

$$\bar{k} = (1-2P_b)l + (Q-1)P_b \tag{A-7}$$

where it is recalled that $Q = 2^n$.

Now consider the quantity

$$\overline{k^2} = \sum_{i=0}^{n-1} \sum_{j=0}^{n-1} \overline{k_i k_j}\, 2^{i+j}; \qquad k = 0, 1, \cdots, Q-1. \tag{A-8}$$

If $i \neq j$ we have $\overline{k_i k_j} = \bar{k}_i \bar{k}_j$ since successive bit transmissions are assumed independent. For $i = j$, on the other hand, we have

$$\overline{k_i^2} = (1-P_{b_i})l_i^2 + P_{b_i}(1-l_i^2) = (1-2P_{b_i})l_i + P_{b_i} \tag{A-9}$$

where we have made use of the fact that $l_i^2 = l_i$. It follows that

$$\overline{k^2} = \sum_{i=0}^{n-1} \{(1-2P_{b_i})l_i + P_{b_i}\}2^{2i}$$

$$+ \sum_{\substack{i=0 \\ i \neq j}}^{n-1} \sum_{j=0}^{n-1} \{(1-2P_{b_i})l_i + P_{b_i}\}\{(1-2P_{b_j})l_j + P_{b_j}\}2^{i+j}, \tag{A-10}$$

whereupon after some algebra this reduces to

$$\overline{k^2} = \sum_{i=0}^{n-1} P_{b_i}(1-P_{b_i})2^{2i} + \bar{k}^2 \tag{A-11}$$

with $\bar{k}$ given by (A-6). In the particular case $P_{b_i} = P_b, i = 0, 1, \cdots, N-1$, this yields

$$\overline{k^2} = \frac{P_b(1-P_b)(Q^2-1)}{3} + [(1-2P_b)l + (Q-1)P_b]^2. \tag{A-12}$$

Finally, in the general case we have

$$E\{(k-l)^2 \mid l\} = \sum_{i=0}^{n-1} P_{b_i}(1-P_{b_i})2^{2i} + \left[\sum_{i=0}^{n-1} P_{b_i}(1-2l_i)2^i\right]^2 \quad \text{(A-13)}$$

It follows that

$$e_n^2/\sigma_e^2 = \Delta^2\left\{\sum_{i=0}^{n-1} P_{b_i}(1-P_{b_i})2^{2i} + \sum_{l=0}^{Q-1}\left[\sum_{i=0}^{n-1} P_{b_i}(1-2l_i)2^i\right]^2 p_l\right\}, \quad \text{(A-14)}$$

and in the particular case that $P_{b_i} = P_b, i = 0, 1, \cdots, n-1$ we have

$$e_n^2/\sigma_e^2 = \Delta^2 P_b(1-P_b)\left\{\frac{(Q^2-1)}{3} + P_b \cdot \sum_{l=0}^{Q-1}[(Q-1)-2l]^2 p_l\right\}. \quad \text{(A-15)}$$

APPENDIX B

EVALUATION OF MUTUAL ERROR TERM

The mutual error term ϵ_m can be expressed as

$$\epsilon_m = \frac{E\{Q_{i,j}N_{i,j}'\}}{\sigma_e^2} = \sigma_e^{-2}E\left\{\sum_{k=-\infty}^{\infty}\sum_{l=-\infty}^{\infty} Q_{i,j}N_{k,l}d_{i-k,j-l}\right\} \quad \text{(B-1)}$$

where $\{N_{i,j}\}$ is the channel noise appearing at the input to the decoder and $\{d_{k,l}\}$ is the 2-D impulse response sequence of the decoder evaluated according to

$$d_{k,l} = \left(\frac{1}{2\pi j}\right)^2 \oint D(z_1, z_2) z_1^{k-1} z_2^{l-1}\, dz_1\, dz_2 \quad \text{(B-2)}$$

with the closed contour integral taken around the unit polydisk in the complex space C^2 possessing coordinates z_1, z_2. Assuming that the channel is memoryless it follows that

$$E\{Q_{i,j}N_{k,l}\} = \delta_{i-k,j-l} \quad \text{(B-3)}$$

with $\delta_{i,j}$ the 2-D impulse sequence defined according to

$$\delta_{i,j} = \begin{cases} 1; & i = j = 0 \\ 0; & \text{elsewhere.} \end{cases} \quad \text{(B-4)}$$

Evaluation of the expectation on the right-hand side of (B-1) yields

$$\epsilon_m = \frac{E\{Q_{i,j}N_{i,j}\}}{\sigma_e^2} d_{0,0} = \frac{E\{Q_{i,j}N_{i,j}\}}{\sigma_e^2}\left(\frac{1}{2\pi}\right)^2 \cdot \int_{-\pi}^{\pi}\int_{-\pi}^{\pi} D(e^{j\lambda_1}, e^{j\lambda_2})\, d\lambda_1\, d\lambda_2. \quad \text{(B-5)}$$

Observe now that

$$\frac{E\{Q_{i,j}N_{i,j}\}}{\sigma_e^2} = \sigma_e^{-2}\sum_{k=0}^{Q-1}\sum_{l=0}^{Q-1}\left\{\int_{E_l}^{E_{l+1}} (\xi - X_l) p_E(\xi)\, d\xi\right\} \cdot (X_k - X_l)P_{k|l} = \Delta\sum_{k=0}^{Q-1}\sum_{l=0}^{Q-1}(k-l)\epsilon_l' P_{k|l} \quad \text{(B-6)}$$

where

$$\epsilon_l' \triangleq \int_{E_l/\sigma_e}^{E_{l+1}/\sigma_e} \{y - [l - (Q-1)/2]\Delta\}\hat{p}_E(y)\, dy; \quad l = 0, 1, \cdots, Q-1. \quad \text{(B-7)}$$

Furthermore, since $\hat{p}_E(\cdot)$ is assumed symmetric it is easily established that

$$\epsilon_l' = -\epsilon_{Q-1-l}'; \qquad l = 0, 1, \cdots, Q/2 - 1. \quad \text{(B-8)}$$

The sum on k appearing on the right-hand side of (B-6) is easily recognized as the conditional expectation of the difference $(k - l)$ given that the l'th level was transmitted. That is

$$E\{(k-l) \mid l\} = \sum_{k=0}^{Q-1}(k-l)P_{k|l} = \bar{k} - l \quad \text{(B-9)}$$

where, as in Appendix A, the overbar indicates conditional expectation given the l'th level was transmitted. From previously established results

$$E\{(k-l) \mid l\} = \sum_{i=0}^{n-1}(1-2l_i)P_{b_i}2^i \quad \text{(B-10)}$$

where again l_i, $i = 0, 1, \cdots, n-1$ represent coefficients in the binary expansion of the integer l and P_{b_i} is the associated bit error probability. It follows that

$$\frac{E\{Q_{i,j}N_{i,j}\}}{\sigma_e^2} = \Delta\sum_{l=0}^{Q-1}\left\{\sum_{i=0}^{n-1}(1-2l_i)P_{b_i}2^i\right\}\epsilon_l'. \quad \text{(B-11)}$$

Now consider performing the summation on l. For each $l = 0, 1, \cdots, Q/2 - 1$ the term within braces will be the negative of that for the index $Q - 1 - l$. From the similar symmetry condition expressed by (B-8) we have

$$\frac{E\{Q_{i,j}N_{i,j}\}}{\sigma_e^2} = 2\Delta \sum_{l=Q/2}^{Q-1} \left\{ \sum_{i=0}^{n-1} (1-2l_i)P_{b_i}2^i \right\} \epsilon_l' \quad \text{(B-12)}$$

so that finally

$$\epsilon_m = 2\Delta \left[\sum_{l=Q/2}^{Q-1} \left\{ \sum_{i=0}^{n-1} (1-2l_i)P_{b_i}2^i \right\} \epsilon_l' \right] \left(\frac{1}{2\pi} \right)^2 \cdot \int_{-\pi}^{\pi} \int_{-\pi}^{\pi} D(e^{j\lambda_1}, e^{j\lambda_2})\, d\lambda_1 d\lambda_2 . \quad \text{(B-13)}$$

ACKNOWLEDGMENT

The authors are indebted to the anonymous reviewers whose comments helped to improve an earlier version of this paper.

REFERENCES

1. D. J. Connor, R. C. Brainard and J. O. Limb, "Intraframe Coding for Picture Transmission", *Proceedings IEEE*, vol. 60, pp. 779-791, July 1972.
2. J. B. O'Neal, "Predictive Quantizing System (Differential Pulse Code Modulation) for the Transmission of Television Signals", *Bell Syst. Tech. J.* vol. 45, pp. 689-721, May-June 1966.
3. D. J. Connor, R. F. W. Pease and W. G. Scholes, "Television Coding Using Two-Dimensional Spatial Prediction", *Bell Syst. Tech. J.*, vol. 50, pp. 1049-1061, March 1971.
4. J. O. Limb and F. W. Mounts, "Digital Differential Quantizer for Television", *Bell Syst. Tech. J.*, vol. 48, pp. 2583-2599, September 1969.
5. J. O. Limb, C. R. Rubinstein and K. A. Walsh, "Digital Coding of Color Picturephone Signals by Element-Differential Quantization", *IEEE Trans. Commun.*, vol. COM-19, pt. 1, pp. 992-1005, December 1971.
6. D. G. Daut, "An Empirical Study of Two-Dimensional Differential Pulse Code Modulation Encoding of Images", M. S. Thesis, Electrical and Systems Engineering Dept., Rensselaer Polytechnic Institute, Troy, N.Y., July 1977.
7. J. Max, "Quantizing for Minimum Distortion", *IEEE Trans. Inform. Theory*, vol. IT-6, pp. 7-12, March 1960.
8. M. D. Paez and T. H. Glisson, "Minimum Mean-Squared-Error Quantization in Speech PCM and DPCM Systems", *IEEE Trans. Commun.*, vol. COM-20, pp. 225-230, April 1972.
9. R. E. Totty and G. C. Clark, "Reconstruction Error in Waveform Transmission", *IEEE Trans. Inform. Theory*, vol. IT-13, pp. 336-338, April 1967.
10. K.-Y. Chang and R. W. Donaldson, "Analysis, Optimization and Sensitivity Study of Differential PCM Systems Operating on Noisy Communications Channels", *IEEE Trans. Commun.*, vol. COM-20, pp. 338-350, June 1972.
11. J. E. Essman and P. A. Wintz, "The Effects of Channel Errors in DPCM Systems and Comparison with PCM Systems", *IEEE Trans. Commun.*, vol. COM-21, pp. 867-877, August 1973.
12. K.-Y. Chang and R. W. Donaldson, "Nonadaptive DPCM Transmission of Monochrome Pictures Over Noisy Communication Channels", *IEEE Trans. Commun.*, vol. COM-24, pp. 173-183, February 1976.
13. T. J. Goblick, Jr., "Theoretical Limitations on the Transmission of Data From Analog Sources", *IEEE Trans. Inform. Theory*, IT-11, pp. 558-567, October 1965.
14. T. J. Goblick and J. L. Holsinger, "Analog Source Digitization: A Comparison of Theory and Practice", *IEEE Trans. on Inform. Theory*, vol. IT-13, pp. 323-326, April 1967.
15. J. A. Stuller and B. Kurz, "Intraframe Sequential Picture Coding", *IEEE Trans. Commun.*, vol. COM-25, pp. 485-495, May 1977.
16. T. Berger, *Rate Distortion Theory: A Mathematical Basis for Data Compression*, Prentice-Hall, Englewood Cliffs, N.J., 1971.
17. D. G. Daut, "Rate-Distortion Function for 2-D Image Model", unpublished R.P.I. report, April 1978.
18. R. G. Gallager, *Information Theory and Reliable Communication*, Wiley, New York, 1968.
19. F. Jelinek, *Probabilistic Information Theory*, McGraw-Hill, New York, 1968.
20. R. J. McEliece, *The Theory of Information and Coding*, vol. 3, *Encyclopedia of Mathematics and Its Applications*, Addison-Wesley, Reading, Mass., 1977.
21. D. Chase, et al., "Multi-Sample Error Protection Modulation Study", TR-76-161, Rome Air Development Center, Air Force Systems Command, Griffiss Air Force Base, New York, May 1976.
22. A J. Viterbi, "Convolutional Codes and Their Performance in Communication Systems", *IEEE Trans. Commun.*, COM-19, pp. 751-772, October 1971.
23. J. P. Odenwalder, "Optimum Decoding of Convolutional Codes", Ph.D. Dissertation, Syst. Sci. Dept., Univ. California, Los Angeles, 1970.
24. K. J. Larsen, "Short Convolutional Codes with Maximal Free Distance for Rates 1/2, 1/3, and 1/4", *IEEE Trans. Inform. Theory*, vol. IT-19, pp. 371-372, May 1973.
25. J. W. Modestino, "Evaluation and Graphical Display of Performance of Viterbi Decoder in Conjunction with Coherent BPSK Modulation on AWGN Channel", TM78-3, Electrical and Systems Engineering Department, Rensselaer Polytechnic Institute, Troy, N.Y., January 1978.
26. J. M. Wozencraft and I. M. Jacobs, *Principles of Communications Engineering*, Wiley, New York, 1965.
27. A. J. Viterbi, "Error Bounds for Convolutional Codes and an Asymptotically Optimum Decoding Algorithm", *IEEE Trans. Inform. Theory*, vol. IT-13, pp. 260-269, April 1967.
28. J. L. Massey, "Coding and Modulation in Digital Communications", *Proc. Int. Zurich Seminar on Digital Communications*, Zurich, Switzerland, March 1974.
29. J. L. Massey, *Course Notes for EE453*, Dept. of Elect. Eng., Univ. of Notre Dame, Indiana, 1976.

★

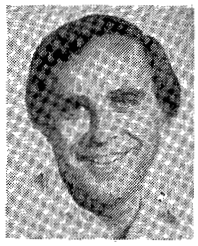

James W. Modestino (S'60–M'69) was born in Boston, MA on April 27, 1940. He received the B.S. degree in Electrical Engineering from Northeastern University, Boston, MA, in 1962, the M.S. degree in electrical engineering from the University of Pennsylvania, Philadelphia, 1964, and the M.A. and Ph.D. degrees from Princeton University, Princeton, NJ, in 1968 and 1969, respectively.

He has held a number of industrial positions including positions with RCA Communication Systems Division, Camden, NJ, AVCO Systems Division, Wilmington, MA, GTE Laboratories, Inc. Waltham, MA and MIT Lincoln Laboratory, Lexington, MA. From 1970 to 1972 he was an Assistant Professor in the Department of Electrical Engineering, Northeastern University. In 1972 he joined Rensselaer Polytechnic Institute, Troy, NY, where he presently is a Professor in the Department of Electrical and Systems Engineering. Here he has been responsible for teaching and research in the communication and information processing systems area. His specific interests include: communication in fading dispersive channels; detection, estimation, and filtering in impulsive noise environments; and digital image processing with particular application to biomedicine.

★

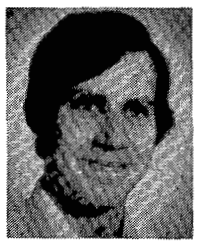

David G. Daut (S'75) was born in Paterson, New Jersey, on October 11, 1954. He received the B.S. degree in electrical engineering from New Jersey Institute of Technology, NJ, in 1976, and the M.S. degree in electrical engineering from Rensselaer Polytechnic Institute, Troy, NY, in 1977.

Since 1976 he has been a Research Assistant in the Department of Electrical and Systems Engineering, Rensselaer Polytechnic Institute, where he is currently studying for the Ph.D. degree. His doctoral research is focused on data/bandwidth compression techniques in the context of image coding and transmission.